Impact of Soil Moisture–Atmosphere Interactions on Surface Temperature Distribution

Alexis Berg
Rutgers University - New Brunswick/Piscataway

Benjamin R. Lintner
Rutgers University

Kirsten L. Findell
Geophysical Fluid Dynamics Laboratory

Sergey Malyshev
Princeton University

Paul C. Loikith
Portland State University, ploikith@pdx.edu

See next page for additional authors

Authors
Alexis Berg, Benjamin R. Lintner, Kirsten L. Findell, Sergey Malyshev, Paul C. Loikith, and Pierre Gentine

Impact of Soil Moisture–Atmosphere Interactions on Surface Temperature Distribution

ALEXIS BERG,*,+ BENJAMIN R. LINTNER,# KIRSTEN L. FINDELL,@ SERGEY MALYSHEV,&
PAUL C. LOIKITH,** AND PIERRE GENTINE++

** Rutgers, The State University of New Jersey, New Brunswick, and Geophysical Fluid Dynamics Laboratory, Princeton, New Jersey*
 # Rutgers, The State University of New Jersey, New Brunswick, New Jersey
@ Geophysical Fluid Dynamics Laboratory, Princeton, New Jersey
& Princeton University, Princeton, New Jersey
*** Jet Propulsion Laboratory, California Institute of Technology, Pasadena, California*
++ Columbia University, New York, New York

(Manuscript received 30 September 2013, in final form 3 May 2014)

ABSTRACT

Understanding how different physical processes can shape the probability distribution function (PDF) of surface temperature, in particular the tails of the distribution, is essential for the attribution and projection of future extreme temperature events. In this study, the contribution of soil moisture–atmosphere interactions to surface temperature PDFs is investigated. Soil moisture represents a key variable in the coupling of the land and atmosphere, since it controls the partitioning of available energy between sensible and latent heat flux at the surface. Consequently, soil moisture variability driven by the atmosphere may feed back onto the near-surface climate—in particular, temperature. In this study, two simulations of the current-generation Geophysical Fluid Dynamics Laboratory (GFDL) Earth System Model, with and without interactive soil moisture, are analyzed in order to assess how soil moisture dynamics impact the simulated climate. Comparison of these simulations shows that soil moisture dynamics enhance both temperature mean and variance over regional ''hotspots'' of land–atmosphere coupling. Moreover, higher-order distribution moments, such as skewness and kurtosis, are also significantly impacted, suggesting an asymmetric impact on the positive and negative extremes of the temperature PDF. Such changes are interpreted in the context of altered distributions of the surface turbulent and radiative fluxes. That the moments of the temperature distribution may respond differentially to soil moisture dynamics underscores the importance of analyzing moments beyond the mean and variance to characterize fully the interplay of soil moisture and near-surface temperature. In addition, it is shown that soil moisture dynamics impacts daily temperature variability at different time scales over different regions in the model.

1. Introduction

Much of the anticipated risk of global warming for human and natural systems is associated with projected changes in the occurrence and intensity of extreme climatic events (Field 2012). Regional increases in the frequency of extreme events, such as heat waves, droughts, and heavy precipitation, coupled with the potentially increased likelihood of event amplitude outside the range experienced in the recent past, may exceed human or ecosystem adaptive capacity and resilience. Quantifying the statistics of such events is inherently challenging, as their frequency of occurrence is small. On the other hand, it is not unreasonable to expect that extreme events may be sensitive to modifications of the probability distribution functions (PDFs) of variables such as temperature and precipitation, especially the tails of the PDFs. An important open question is whether, in the context of climate change, changes in

+ Current affiliation: International Research for Climate and Society (IRI), The Earth Institute at Columbia University, Palisades, New York.

Corresponding author address: Alexis Berg, International Research for Climate and Society (IRI), The Earth Institute at Columbia University, 61 Rt. 9W, Palisades, NY 10964.
E-mail: aberg@iri.columbia.edu

DOI: 10.1175/JCLI-D-13-00591.1

extremes simply result from a shift in the mean of the distribution, or whether changes in higher-order moments, controlling the shape of the PDF, also contribute to changes in the occurrence of extreme events [e.g., refer to figure SPM.3 in Field (2012) and to Seneviratne et al. (2012)]. With respect to the evolution of extreme events over the twentieth century, regional studies indicate conflicting results (e.g., Griffiths et al. 2005; Simolo et al. 2011; Ballester et al. 2010). Rhines and Huybers (2013) suggest that observational evidence of changes in the frequency of extreme hot summers can be explained by a simple shift in the mean without changes in the shape of the PDF, given currently available data. Donat and Alexander (2012), on the other hand, presented observational evidence of increasing variance and skewness of the distribution of daily surface temperature at the global scale, suggesting that changes in temperature PDFs already play a role in changes in temperature extremes.

In addition, Ruff and Neelin (2012) recently demonstrated how projection of future changes in temperature extremes (defined as threshold exceedance) is sensitive to the details of the present-day PDF tails: that is, whether the tails are Gaussian or non-Gaussian leads to different estimates of expected change. Therefore, because changes in climate extremes result from the combination of present-time PDF characteristics and how they will evolve in the future, accurate projection of the effect of climate change on extremes requires understanding of the underlying physical processes shaping these distributions. Linking PDF shapes to physical processes has been the focus of some recent studies in climate science (Neelin et al. 2010; Ruff and Neelin 2012; Loikith and Broccoli 2012; Loikith et al. 2013). Such studies have typically focused on atmospheric processes; for example, Loikith and Broccoli (2012) investigate synoptic patterns associated with the tails of the temperature distribution over North America. Here, we extend this line of research by investigating the impact of land–atmosphere interactions on the distribution of daily surface temperature at the global scale with a focus on the role of soil moisture–atmosphere feedbacks.

Soil moisture is a key variable in land–atmosphere interactions: the variations of soil moisture in response to atmospheric conditions (precipitation, radiation, and evaporative demand) impact surface turbulent and radiative heat fluxes, thereby potentially feeding back on atmospheric conditions. For example, low precipitation conditions can ultimately limit soil moisture availability, leading to decreased latent and increased sensible heating at the surface. Attendant increases in atmospheric temperature and impacts on boundary layer structure and thermodynamics may render the atmosphere less conducive to precipitating deep convection, resulting in a reinforcement of, or positive feedback on, low precipitation (Findell and Eltahir 2003a,b; D'Odorico and Porporato 2004; Findell et al. 2011; Gentine et al. 2011, 2013).

Soil moisture–atmosphere interactions have been the subject of numerous studies [for a review, see Seneviratne et al. (2010)]. Because of the relative paucity of soil moisture and land–atmosphere flux measurements at the necessary spatial and temporal scales, as well as the difficulty in isolating causality in observations of the coupled land–atmosphere system (Findell et al. 2011; Orlowsky and Seneviratne 2010), investigation of these processes has often relied on modeling. Setting aside the obvious caveats regarding model fidelity, a frequently used approach involves comparing control simulations with simulations in which soil moisture is prescribed (Koster et al. 2002, 2004; Seneviratne et al. 2006; Conil et al. 2007; Krakauer et al. 2010); in the latter, soil moisture is prevented from responding to the atmosphere, thus severing the feedback loop between soil moisture and the atmosphere. Such studies have generated the notion of ''hotspot'' regions in which land–atmosphere interactions significantly enhance surface temperature and precipitation variability, although the magnitudes and spatial patterns of this coupling vary substantially between models and with model resolution (e.g., Koster et al. 2006; Hohenegger et al. 2009; Seneviratne et al. 2010). In addition, soil moisture–atmosphere coupling has been shown to play a determining role in climate extremes, such as floods and heat waves (Paegle et al. 1996; Pal and Eltahir 2003; Fischer et al. 2007). Recent model and observational studies in particular suggest that soil moisture–atmosphere feedbacks can affect the tails of temperature distributions (e.g., Jaeger and Seneviratne 2011; Hirschi et al. 2011; Mueller and Seneviratne 2012). Such local land–atmosphere processes may thus be expected to contribute to shaping the PDFs of different surface climate variables (Diffenbaugh et al. 2005).

Many of the studies alluded to above have emphasized soil moisture–induced changes in variable dispersion (e.g., standard deviation): as such, they have not fully evaluated the effect of soil moisture dynamics on the overall distribution shapes of these climate variables. Here, we note that measures like the standard deviation may provide a poor basis for assessing how the tails of the PDFs will respond to a forcing. Given the importance of understanding the governing processes of climate PDFs and associated distribution tails, as outlined above, we perform here a complete assessment of the impact of soil moisture dynamics on the distribution of daily surface temperature. To do so, we consider changes in all moments of the temperature PDF between simulations with and without interactive soil moisture. The remainder of this paper is organized as follows: Section 2 presents the model and experimental setup used for these simulations. Section 3 exposes the results of the different simulations in terms of temperature distribution and the processes responsible for these differences. Section 4 includes some further discussion and conclusions.

2. Methods

As part of phase 5 of the Coupled Model Intercomparison Project (CMIP5) Global Land–Atmosphere Coupling Experiment (GLACE-CMIP5) model intercomparison project (Seneviratne et al. 2013), simulations were performed with the Geophysical Fluid Dynamics Laboratory (GFDL) Earth System Model with the Modular Ocean Model (ESM2M; Dunne et al. 2012) over 1951–2100, with and without interactive soil moisture. In both cases, historical radiative forcing agents [well-mixed greenhouse gases (CO_2, CH_4, N_2O, and halons), tropospheric and stratospheric O_3, aerosol concentrations (sulfate, black and organic carbon, sea salt, dust, and volcanic aerosols), solar irradiance, and land use transitions] were prescribed over 1951–2005, while the representative concentration pathway RCP8.5 was assumed thereafter. Moreover, sea surface temperatures (SSTs) and sea ice concentrations over the whole simulation were prescribed in each simulation from a fully coupled (ocean–atmosphere) concentration-driven simulation originally performed with ESM2M in support of CMIP5. ESM2M uses the Atmospheric Model, version 2 (AM2) with a 2° latitude × 2.5° longitude horizontal grid with 24 vertical levels, on a D grid using finite-volume advection (Lin 2004) with a 30-min dynamical time step and 3-h radiation time step. The atmospheric physical parameterizations are described in GFDL Global Atmospheric Model Development Team (2004). The coupled land model component is GFDL's Land Model, version 3 (LM3), described by Milly et al. (2014). LM3 includes multilayer representations of temperature, liquid water content, and ice content of snowpack and of the soil–bedrock continuum; horizontal transport of runoff to the ocean via a global river network; and lakes, lake ice, and lake-ice snow packs that exchange mass and energy with both the atmosphere and the rivers. Vegetation dynamics and biophysics are interactively computed in LM3 as in the model LM3V (Shevliakova et al. 2009).

In the interactive soil moisture case [the control simulation (CTL)], soil moisture dynamics responds to atmospheric variability (e.g., precipitation or evaporative demand). In the prescribed soil moisture case (denoted simulation 1A), soil moisture is overridden at each time step, in each of the 20 soil layers, by its climatological value computed for each pixel over 1971–2000 from the original coupled simulation; monthly soil moisture climatological values are linearly interpolated in order to prescribe values at each time step in the model. A difference of this experiment from the first GLACE experiment (Koster et al. 2004) is that, in the prescribed case here, soil moisture is overridden by climatological values (from the 30-yr period 1971–2000) and not directly by soil moisture outputs from the interactive run [thus, similar to the approach used in Seneviratne et al. (2006)]. The implications of this particular protocol are discussed in section 4. Here, we compare the two simulations over 1971–2000; focusing on this time period ensures that both simulations have identical soil moisture climatologies. The comparison thus isolates the effect on climate of soil moisture–atmosphere interactions, as these interactions are active in CTL and effectively disabled in 1A, since soil moisture does not respond to the atmosphere in this simulation. Since land–atmosphere coupling is generally expected to be stronger in summer (Dirmeyer 2003), our analysis considers distributions of daily-mean near-surface temperature in boreal summer [June–August (JJA)].

Comparing distributions of climate variables on the global scale is practically challenging, since the PDFs are difficult to visualize over all pixels at the same time. Thus, in order to analyze the changes in the distribution of daily temperatures and other surface variables globally, we calculate and compare over each pixel the first four moments of the distribution: mean, standard deviation, skewness, and kurtosis. While a distribution is, in general, not entirely characterized by these four moments, moment changes between both simulations provide a first quantitative assessment of the overall change in the aspect of the distribution. While the standard deviation measures the dispersion of a distribution (i.e., the variability) around its location (i.e., mean), higher-order moments characterize the shape of the PDF. Skewness measures the asymmetry of the tails from both sides of the distribution, with positive (negative) skew indicating the presence of a longer tail on the high (low) end of the distribution, while the kurtosis assesses how much of the distribution lies in the peak around the mean and in the tails, compared to the "shoulders" in between. That is, a distribution with a high peak around the mean, long tails, and little in between will have a higher kurtosis than a squat distribution with a low peak and short tails. In addition to analyzing changes in distribution moments, we also investigate in more detail

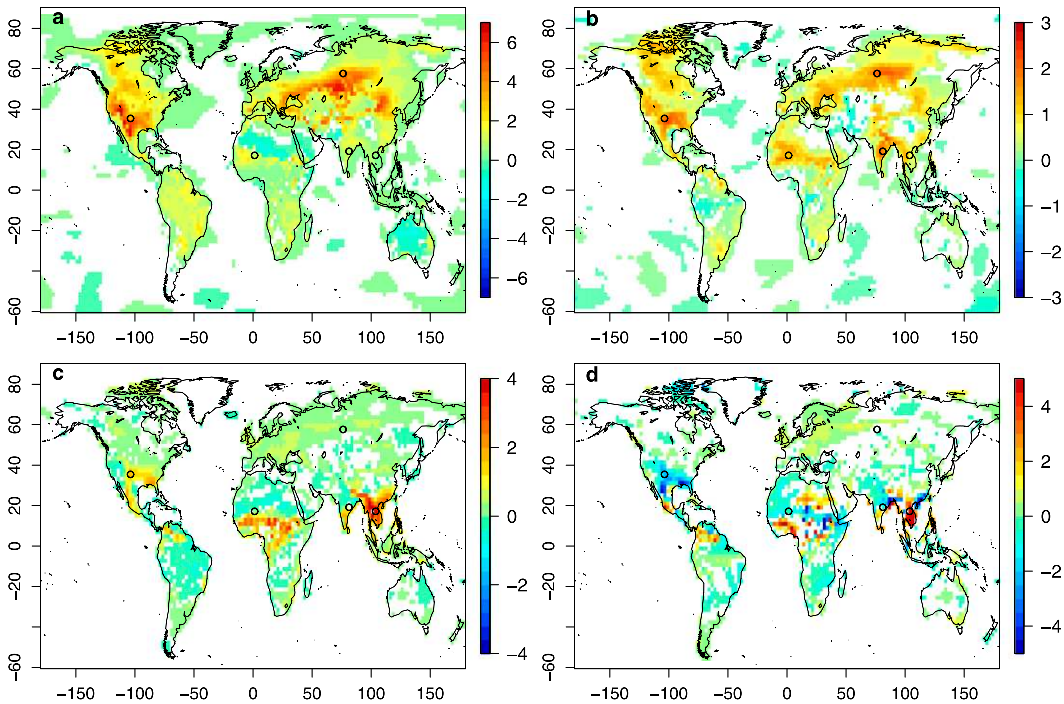

FIG. 1. Difference of the four first moments of the distribution of daily JJA 2-m temperature between simulations CTL and 1A (CTL − 1A) over 1971–2000: (a) mean (K), (b) standard deviation (K), (c) skewness (unitless), and (d) kurtosis (unitless). Pixels with no significant difference at the 1% level between both simulations were blanked out, according to the following tests: for the mean, a Welch test (which does not assume equal variance); and for the standard deviation, a Levene test (which does not assume normal distribution of the data). For the skewness and kurtosis, a test was designed as follows: for each pixel, the two distributions (daily temperature from 1A and from CTL) were concatenated, shuffled randomly, and redrawn 1000 times; differences in skewness and kurtosis were estimated to be significant when they were greater (lower) than the 95% (5%) quantile of the corresponding distribution of differences. Note that for kurtosis in (d), the color scale saturates at −5/5 for greater legibility. Panels (c) and (d) are shown over land only. Black circles indicate the five points used in Figs. 2, 3, and 7: in the United States, the Sahel, central Asia, India, and Southeast Asia.

the PDFs of surface–atmosphere variables for representative spatial locations in order to gain insights into the operation of regional-scale processes and how these may differ geographically.

3. Results

a. *Changes in temperature distribution*

We first highlight differences in daily temperature distribution between both simulations over 1971–2000 by considering the first four moments of the distribution (Fig. 1). Figure 1a indicates that a leading-order impact of soil moisture dynamics and associated feedbacks to the atmosphere is to increase average JJA temperature over some regions of the Northern Hemisphere, with peak values of 7 K over parts of North America and central Asia. By contrast, mean temperature appears to change only modestly over the tropics. Moreover, in really dry regions (e.g., the Sahara), a small cooling can be noted. Similar changes in mean JJA temperature were documented in analogous model experiments with the Goddard Institute for Space Studies Model (GISS) in Krakauer et al. (2010), albeit with smaller amplitude. This difference in the strength of the effect is likely due to different treatment of vegetation in the two models (interactive vs prescribed, discussed more below). Figure 1b further shows that the shift in mean near-surface air temperature over North America and central Asia is associated with a large increase in temperature standard deviation in summer, by up to 3 K; in addition, tropical monsoon regions like India and the Sahel also display a significant increase in JJA daily temperature variability. Such regions of enhanced temperature standard deviation can be understood as regions of strong soil moisture–temperature coupling, in the sense that soil moisture–atmosphere interactions contribute strongly to the variability in summertime surface temperature. Areas of enhanced variability identified here are consistent with many of the hotspot regions highlighted in previous assessments of soil moisture–temperature coupling, either based on modeling experiments similar to the one performed here (Koster et al. 2006; Seneviratne et al. 2006) or based on observations [Mueller and Seneviratne (2012); Miralles et al. (2012), Fig. 1 therein].

Figures 1c and 1d further reveal that soil moisture dynamics have a profound impact not only on the dispersion of simulated surface temperature, but also on the shape of the corresponding PDFs. Skewness generally increases in CTL compared to 1A (Fig. 1c), indicating that interactive soil moisture displaces the core of the temperature distribution to the left (relative to the new, warmer mean) and widens the high-side tail. This effect is particularly pronounced over the Southeast United States, the southern fringe of the Sahel, and Southeast Asia. Although the signal is more heterogeneous, kurtosis generally decreases over the same regions (Fig. 1d)—in particular over the Southeast United States—meaning that the corresponding temperature distribution peaks tend to be suppressed and the distribution shoulders become heavier. However, some regions conversely show increasing kurtosis (Southeast Asia and the Sudanian part of West Africa). Importantly, some regions exhibiting pronounced enhancement of temperature standard deviation do not manifest strong differences in either skewness or kurtosis (central Asia and India), while others show strong differences in terms of PDF shape without large changes in standard deviation or mean (Southeast Asia). This underscores the importance of analyzing higher-order moments of variability in order to fully assess the impacts of soil moisture–atmosphere interactions on near-surface temperature.

To provide more insight into these changes in moments, Fig. 2 shows the temperature distributions in CTL and 1A over five points taken as representative examples of the regions and behaviors mentioned above (see points on Fig. 1). While considering individual grid cells may limit the spatial interpretation of the analyzed pixels, it allows for clearly highlighting the PDF behavior, as well as the processes involved (see section 3b). In general, the CTL temperature distributions contain a high-side shoulder relative to 1A, albeit with some regional differences, which are reflected in the distinct changes in the various moments of the distribution over these regions. Over the points in the central United States and central Asia, this shoulder is large enough to substantially alter the distribution mean, while over the three other points highlighted, the impact on the mean is limited. The high-side shoulder in CTL is associated with increased standard deviation everywhere, except over Southeast Asia, where the associated high-side tail is so flat that it leads to a strong increase in skewness

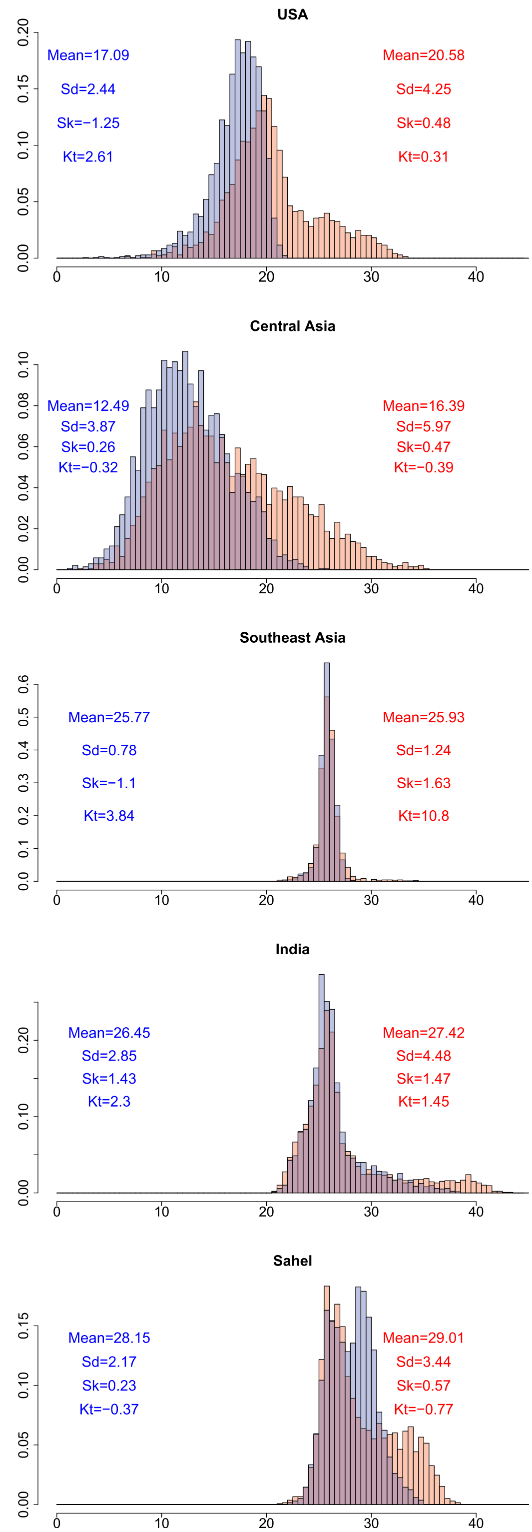

FIG. 2. Distribution of daily JJA 2-m temperatures over the five points shown on Fig. 1, for CTL (red) and for 1A (blue). The *y* axis shows histogram densities. The legend indicates the values of the first four moments of the corresponding distributions: mean, standard deviation (Sd), skewness (Sk), and kurtosis (Kt).

(i.e., asymmetry of the tails) but comparatively little change in standard deviation. A strong increase in skewness is further evident over the central U.S. point, whereas over points in India, the Sahel, and central Asia, skewness is little affected. In general, flatter and more spread out PDFs in CTL are associated with lower kurtosis, although the strength of this effect varies from strong (central United States) to weak (central Asia). Over Southeast Asia, the very large increase in kurtosis (see also Fig. 1d) results from the very sharp high-side tail in CTL, which actually increases the overall weight of the tails in the distribution.

Overall, Fig. 2 indicates that the changes in distribution moments primarily correspond to changes occurring on the high side of the temperature distribution. In contrast, apart from slight increases in the number of low-temperature days over either the Sahel or India, summertime low temperatures are effectively unchanged by interactive soil moisture. That soil moisture–atmosphere interactions disproportionately impact the high side of the temperature distribution underscores how such interactions may be especially critical for high temperature extremes (see also Hirschi et al. 2011; Mueller and Seneviratne 2012). In the following section, we focus on the physical processes linking the difference in soil moisture variability between both simulations to regional differences in the temperature PDFs.

b. *Physical processes*

In general, one may expect the prescription of soil moisture to impact surface temperature through changes to surface turbulent heat fluxes, both directly through the impact of surface heat flux partitioning on surface temperature and indirectly through the impact of surface fluxes on boundary layer processes, cloud cover, and radiation (Betts et al. 2004; Betts and Viterbo 2005; Betts 2007; Gentine et al. 2010, 2013; Seneviratne et al. 2010; Lintner et al. 2013). To highlight the surface processes at play, Fig. 3 depicts distributions of surface energy fluxes in both simulations over the same points analyzed in Fig. 2.

1) GENERAL MECHANISM TO ACCOUNT FOR THE DIFFERENCE BETWEEN INTERACTIVE AND PRESCRIBED SOIL MOISTURE

The general mechanism inferred from Fig. 3 is as follows: in CTL, interactive soil moisture dynamics induces greater soil moisture variability and, thus, a wider distribution of soil moisture compared to the climatology imposed in 1A. In particular, interactive soil moisture permits the development of very dry conditions (Fig. 3a) [here and in the following we use surface soil moisture (first 10 cm), as it is more strongly correlated to heat fluxes than the total 10-m column moisture]. Thus, evapotranspiration in CTL is more frequently soil moisture–limited, as depicted in the relationship between soil moisture and the evaporative fraction (EF), which is the ratio of latent heat flux to the sum of sensible and latent heat fluxes (Fig. 3a). In general, this relationship is characterized by two regimes: a moisture-limited regime in which available surface energy exceeds the amount needed to evaporate or transpire the available moisture, so EF increases with soil moisture; and an energy-limited regime, in which moisture is abundant and EF saturates with respect to increasing soil moisture [Gentine et al. (2011); see also Fig. 5 in Seneviratne et al. (2010)]. Here, in CTL more days typically lie in the moisture-limited portion of the relationship, while in 1A, because soil moisture is prescribed to climatological values, more days lie in the energy-limited regime. Increasing soil moisture limitation in CTL leads to increasing frequency of days with low evapotranspiration in CTL (Fig. 3b) and thus a corresponding increase in days with high sensible heat flux (Fig. 3c). Higher sensible heat fluxes lead to elevated surface temperature; hence, as is evident from the comparison of Fig. 3c and Fig. 2, the resulting differences in the sensible heat flux distribution strongly determine the differences in temperature distribution. In other words, specific changes in moments of the temperature distribution over different regions [i.e., different combinations of changes in mean, variance, skewness, and kurtosis associated with the emergence of a high-side shoulder in the distribution in CTL (discussed in section 3a)] appear to reflect how the PDFs of surface heat fluxes are affected by interactive versus prescribed soil moisture. Note that differences in surface heat fluxes are also associated with differences in the distribution of cloud cover and thus incoming solar radiation (Fig. 3d), which may further contribute to differences in temperature distribution by altering available surface energy.

In the following subsections, we diagnose some of the principal regional differences in the general mechanism discussed here; that is, we consider the impacts of soil moisture dynamics on land–atmosphere fluxes that lead to the distinct regional changes in the temperature PDFs.

2) CENTRAL UNITED STATES AND CENTRAL ASIA

The North American and central Asian points reflect regions of large increase in the mean temperature in Fig. 1a. Figure 3 shows that over these two points the soil moisture limitation mechanism described above is strong enough to decrease mean evapotranspiration (Fig. 3b, first two rows) and increase mean sensible heat flux (Fig. 3c), as well as to increase mean incoming

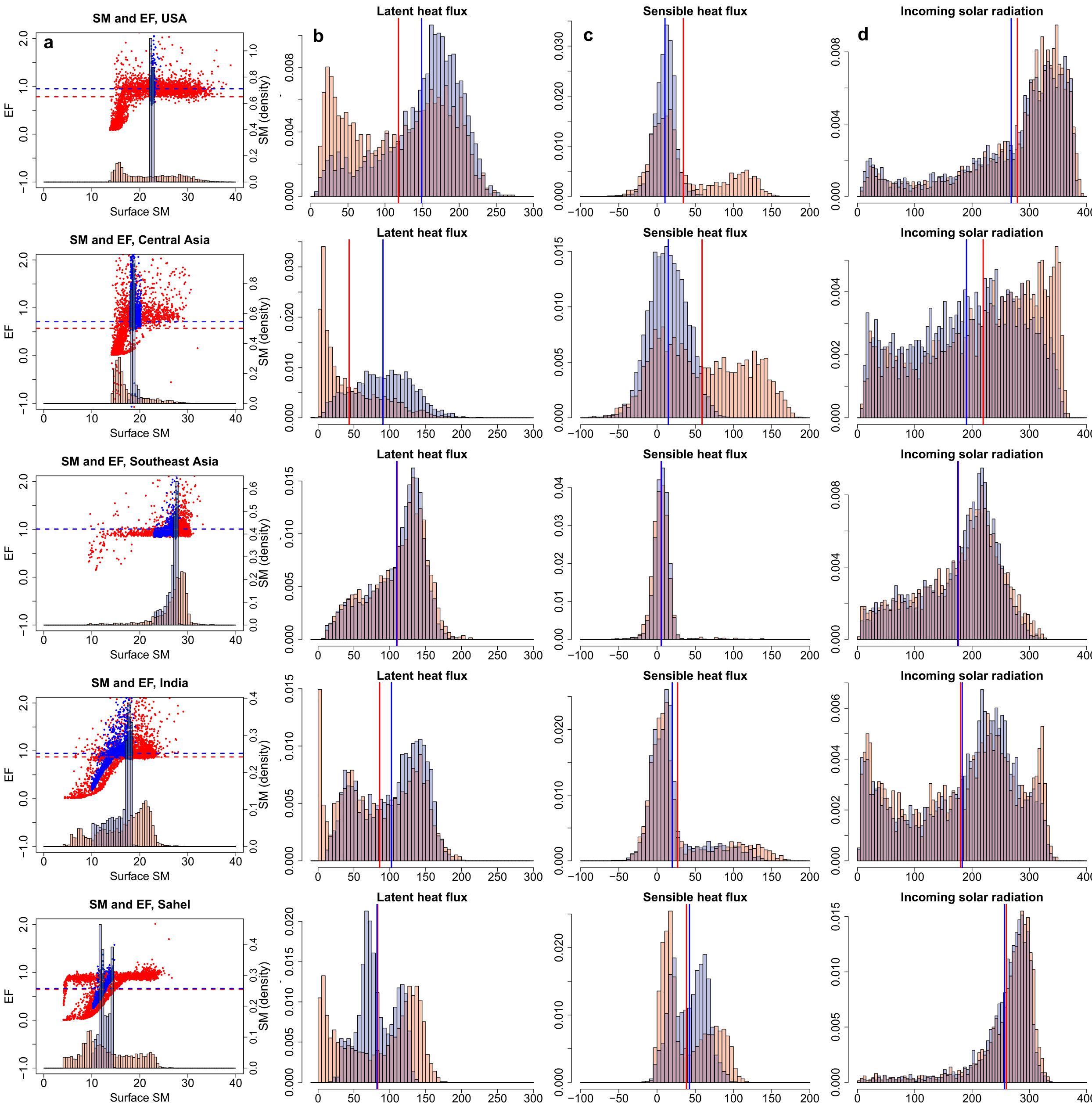

FIG. 3. Over (top to bottom) the same five points as Fig. 2, for CTL (red) and 1A (blue), using JJA values over 1971–2000: (a) dots represent daily EF (left axis) as a function of daily surface soil moisture; horizontal dashed lines represent average EF; and histograms represent distribution of daily surface soil moisture values (SM; right axis). Daily distributions of (b) latent heat flux, (c) sensible heat flux, and (d) incoming shortwave radiation; vertical bars represent the mean of the distribution. Right *y* axis on (a) and *y* axes on (b),(c), and (d) represent histogram densities.

radiation (Fig. 3d). These changes account for the pronounced mean warming in CTL over these two regions. By contrast, the other points in Fig. 3 do not show appreciable mean shifts in the PDFs of the surface energy budget terms.

The decreased evaporative fraction over North America and central Asia in CTL is attributable to the characteristics of the interactive soil moisture distribution compared to the climatological distribution, and how these respective distributions then convolute with the nonlinear soil moisture–EF relationship. The North American and central Asian points are dry in summer (mean JJA rainfall of 4.1 and 1.3 mm day^{-1}, respectively), with frequent dry days punctuated by rainy days;

therefore, over these regions, soil moisture dynamics induce a strongly positively skewed distribution of soil moisture values, with far more numerous low soil moisture anomalies than high ones (Fig. 3a). As a result, in CTL, EF is commonly low, reflecting a soil moisture–limited regime. However, in simulation 1A, the corresponding climatological soil moisture values are adequately high to ensure that EF lies entirely in the energy-limited regime, with little sensitivity to soil moisture (Fig. 3a). In other words, in these regions, overriding soil moisture with the climatological seasonal cycle effectively removes the soil moisture limitation on evapotranspiration. One may note that in that case the shape of the latent heat flux PDF (Fig. 3b) directly reflects that of incoming radiation (Fig. 3d). As a result of this difference in evaporative regime (soil moisture– or energy-limited), the average difference in EF between both simulations is maximized (cf. horizontal dashed bars on Fig. 3a and vertical bars on Figs. 3b,c). Note that this decrease in evapotranspiration directly reflects a large decrease in vegetation (not shown on Fig. 3); since vegetation is interactively simulated in GFDL ESM2M, the positively skewed soil moisture distribution in CTL leads to a large decrease in vegetation over these regions, as it is associated with increased water stress for vegetation. The decrease in total evapotranspiration thus directly corresponds to a decrease in transpiration from vegetation. Finally, large mean changes in surface fluxes over these two regions between 1A and CTL are also associated with impacts on the simulated boundary layer and cloudiness: warmer days with reduced evapotranspiration in CTL and higher sensible heat flux tend to be associated with reduced low-level cloud cover (not shown) and thus increased mean incoming shortwave radiation (Fig. 3d). Although it is not straightforward to disentangle the respective contributions of each factor contributing to the mean surface warming, increased radiation arguably leads to further warming of the surface (i.e., it is a positive feedback).

Over both central Asia and North America, the raising of sensible heat flux by soil moisture dynamics in CTL compared to 1A leads to a wider distribution of temperature. The corresponding widening of the temperature distribution is thus associated with increased standard deviation. Over the central United States, soil moisture dynamics clearly generates bimodal distributions of latent and sensible heat fluxes. The mode of high sensible heat flux values leads to a more asymmetric and flatter temperature distribution (i.e., increased skewness and decreased kurtosis). Note that the mapping between the sensible heat flux and temperature PDFs is not 1:1 (i.e., larger-scale atmospheric processes contribute to temperature variability so that the latter is smoother compared to the former). In addition, because evapotranspiration is consistently energy limited in 1A over that point, the distribution of temperature in 1A does not reflect that of sensible heat flux, but rather the PDF of incoming radiation (Fig. 3d). This accounts for the negative skewness of the temperature PDF in 1A (Fig. 2), which thus exacerbates the skewness difference between both simulations in terms of temperature (compared to the skewness difference of the sensible heat flux PDFs).

Because it is even drier, the point in central Asia displays a more skewed interactive soil moisture distribution than the central U.S. point. As a result, the latent heat flux distribution in CTL, instead of becoming bimodal, becomes strongly positively skewed, with a single peak at very low values. This results in a squatter PDF of sensible heat flux compared to the central U.S. point, with little bimodality. Ultimately, this change in sensible heat distribution leads to a PDF of temperatures that exhibits an increase in standard deviation compared to simulation 1A but, contrary to the U.S. point, little change in the overall shape of the PDF, its skewness, or kurtosis (see Fig. 2). In other words, over central Asia, simulations 1A and CTL exhibit similar temperature PDF shapes for distinct reasons: in CTL, the shape largely resembles that of the sensible heat flux distribution, whereas in 1A, where soil moisture limitation is alleviated, the temperature PDF resembles that of incoming radiation (Fig. 3d). Note that the radiation PDF is not as negatively skewed here as over the point in North America; this reflects the enhancement of cloud cover as a result of increased evapotranspiration in 1A, which truncates the high side of the radiation distribution. The relative invariance of temperature skewness or kurtosis between CTL and 1A thus appears to stem from a trade-off between soil moisture and cloud radiative processes.

3) India and Southeast Asia

In contrast to the central U.S. and central Asia points, the representative points in India and Southeast Asia lie mostly in the energy-limited EF regime in both simulations. Southeast Asia and India are wetter points, where JJA corresponds to the rainy season (mean JJA precipitation of 8.8 and 12.5 mm day^{-1}, respectively, in CTL). Since rainfall is frequent, soil moisture in the interactive case is negatively skewed, with many small positive anomalies (on rainy days) and a few large negative corresponding to occasional dry spells (Fig. 3a). Since both simulations lie mostly in the energy-limited regime, in which surface fluxes do not depend on soil moisture variations, the wider distribution of soil moisture values in the interactive case does not impact surface heat fluxes enough to alter their mean values strongly.

The behavior of the point in Southeast Asia is illustrative of the wettest case in which soil moisture variability can influence temperature distribution: in the interactive case, only a few days fall in the soil moisture–limited regime, which are associated with lower evapotranspiration and higher sensible heat flux. This leads to the very flat tail of high temperature (Fig. 2), which is not associated with large changes in the mean or the standard deviation but a very strong increase in skewness and kurtosis, as discussed in section 3a. The point over India behaves in essentially the same way, except that the local climate there in the 1A simulation lies in the soil moisture–limited regime during part of JJA, leading to a flat high-side tail of sensible heat flux values and temperatures in 1A: in particular, this regime corresponds to the month of June, when the summer monsoon is not yet fully established over South Asia, so climatological soil moisture is still low and vegetation growth is limited. In the interactive case, soil moisture limitation is further enhanced, leading to a more pronounced high-side tail of sensible flux (Fig. 3c) and temperature (Fig. 2). This is associated with increased standard deviation but little change in skewness, as simulation 1A is already heavily skewed.

4) Sahel

Similarly to the central United States, the Sahel is a dry region (mean JJA rainfall of 4.3 mm day^{-1} in CTL). As explained above, interactive soil moisture thus leads to a positively skewed soil moisture distribution; but contrary to the central U.S. or central Asia points, climatological soil moisture in simulation 1A in JJA remains too low to relieve soil moisture limitation, and EF remains essentially soil moisture limited (Fig. 3a). Simulation 1A exhibits delays in vegetation phenology compared to the interactive case (not shown); in CTL, in certain years early rainfall events yield sufficient soil moisture for vegetation to begin growing in the model, while in 1A, the soil moisture evolution is smoothed out so that vegetation growth initiates later. As a result, over JJA mean leaf area index (LAI) is actually slightly lower in 1A (although it is larger in subsequent months). Note that the dual-phase soil moisture–EF relationship in Fig. 3a for the Sahel illustrates this behavior of vegetation: the s-shaped phase (in CTL and 1A) for low soil moisture values corresponds to conditions under which vegetation has not yet developed in the model and only soil evapotranspiration takes place, while the high-evapotranspiration phase for similar low soil moisture values (in CTL only) reflects the presence of transpiring vegetation. In total, because evapotranspiration remains soil moisture–limited in 1A over the Sahel, the wider distribution of soil moisture values in CTL enhances both low and high values of latent and sensible heat flux so that the resulting mean fluxes are not changed (Figs. 3b,c). As a result, the mean temperature remains unchanged.

The increase in the frequency of both high and low latent, and thus sensible, heat flux values leads to a few more days with low temperatures and a large shoulder of high temperatures. This is reflected in the increase in standard deviation, reduced kurtosis, and slightly enhanced skewness of the temperature distribution.

5) Global analysis

Figure 4 extends conclusions from Fig. 3 regarding mean temperature changes to the global land area. One can note the tight overlap between the increase in average temperature (Fig. 1a) and the reduction (increase) in average summertime latent (sensible) heat flux (Figs. 4a,b), which are also concomitant with reduced LAI (Fig. 4c). We speculate that this decrease in vegetation explains the greater temperature change in our simulations compared to those in the similar experiment by Krakauer et al. (2010), in which vegetation was prescribed. Consistent with the discussion of Fig. 3, low-latitude regions in the Northern Hemisphere show little change in average summertime turbulent fluxes, in contrast to either North America or central Asia. Furthermore, the higher near-surface temperature and reduced specific humidity in CTL (from reduced evapotranspiration) leads to a greater potential evapotranspiration (Fig. 4d); consequently, the greater atmospheric demand further contributes to soil moisture depletion and lower evapotranspiration. In other words, through the complementary relationship between potential and actual evapotranspiration (Bouchet 1963), a positive feedback exists between soil moisture depletion and temperature increase. On the other hand, in extremely arid regions (e.g., Sahara), simulated evapotranspiration is actually slightly higher in CTL (Fig. 4a). In such regions, appreciable latent heat flux only occurs after peaks in soil moisture following rain events in CTL; however, such peaks are absent with average soil moisture conditions prescribed in 1A. Thus, little evapotranspiration takes place in 1A, and temperature then remain warmer on average than in CTL. Finally, Figs. 4e,f confirm that, globally, regions of reduced mean evapotranspiration in CTL tend to be associated with reduced mean cloud cover and, thus, increased incoming shortwave radiation. Changes in cloud cover primarily correspond to changes in low-level clouds (not shown) and are collocated with or located slightly downwind (in a mean low-level sense) from the principal areas of evapotranspiration difference between CTL and 1A; this points to an essentially positive impact of land surface

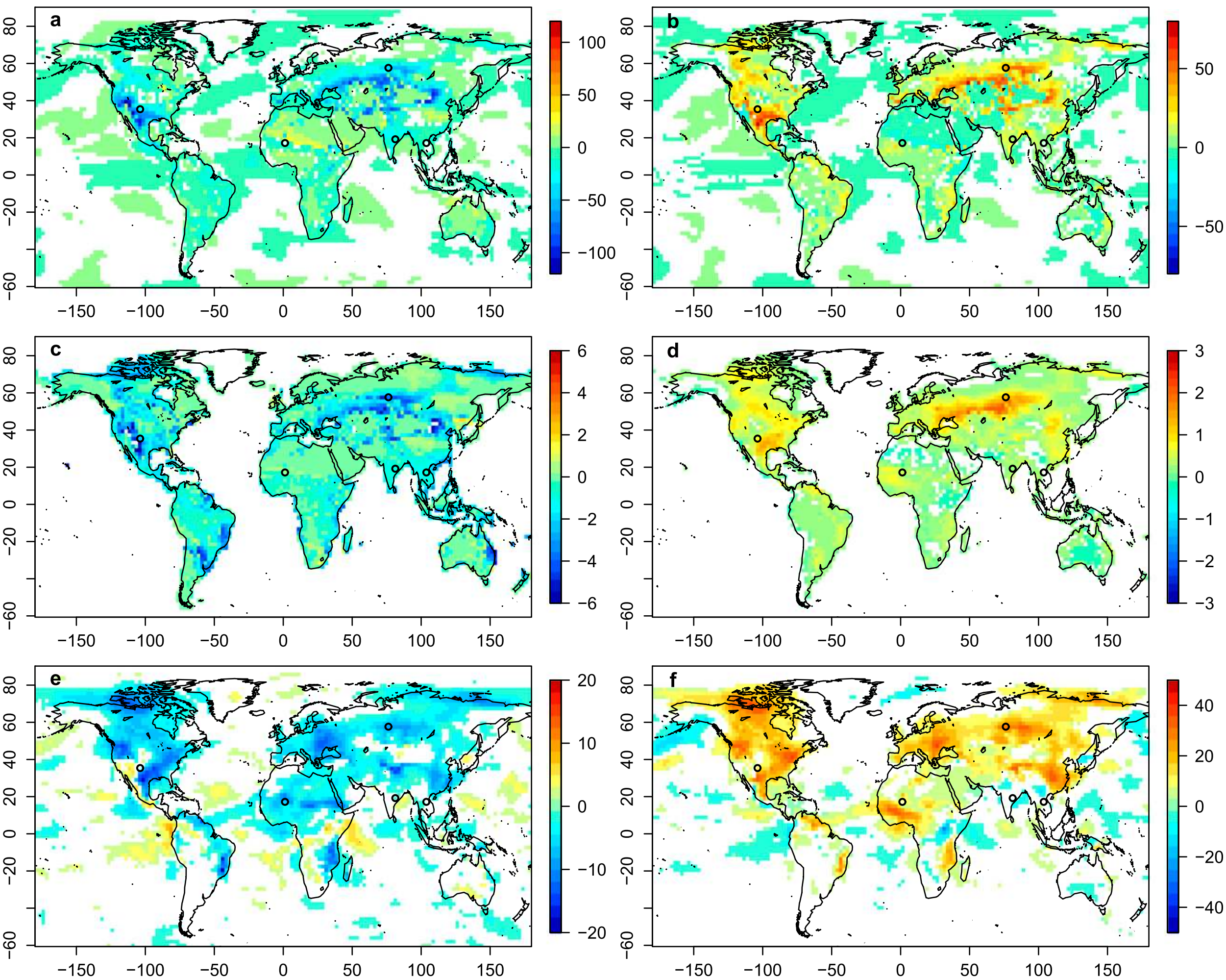

FIG. 4. Difference between JJA daily mean of (a) latent heat flux ($\mathrm{W\,m^{-2}}$); (b) sensible heat flux ($\mathrm{W\,m^{-2}}$); (c) leaf area index; (d) potential evapotranspiration over land, as estimated from model outputs using the Penman–Monteith equation ($\mathrm{mm\,day^{-1}}$); (e) cloud cover (%); and (f) incoming shortwave radiation ($\mathrm{W\,m^{-2}}$) between simulations CTL and 1A (CTL − 1A) over 1971–2000. In all but (c), pixels with no significant difference at the 1% level between both simulations were blanked out (according to a Welch test, which does not assume equal variances).

latent heat flux on regional low-level cloud cover in the model through reduction of the boundary layer humidity (Gentine et al. 2013). One exception is the eastern Sahel region, where surface evapotranspiration is little changed. Here, the reduction in total cloud cover actually corresponds to a change in high-level rather than low-level cloudiness and is therefore not associated with strong insolation changes at the surface (Fig. 4f). As mentioned above, in regions like the Southeast United States and central Asia, the increase in incoming radiation likely feeds back positively on the mean surface warming.

Figure 5 extends the analysis of changes in higher-order moments globally. The tight spatial overlap between Figs. 5a,b,c and Figs. 1b,c,d further confirms the analysis of Figs. 2 and 3 by showing that, globally, the CTL minus 1A differences in the analyzed moments of the temperature distribution over different regions largely mirror changes in moments of surface sensible heat flux PDF. Together, Figs. 3 and 5 show that the generally higher standard deviation, higher skewness and lower kurtosis of the temperature distribution in CTL directly reflect the emergence of positive (negative) anomalies of sensible (latent) heat flux as a result of soil moisture dynamics. Compared to the more atmosphere-driven regime of surface fluxes in simulation 1A, these changes reflect the additional control of soil moisture on evapotranspiration in CTL and thus vary across regions depending on local temperature and precipitation characteristics and associated soil moisture distribution. Although cloud cover variability

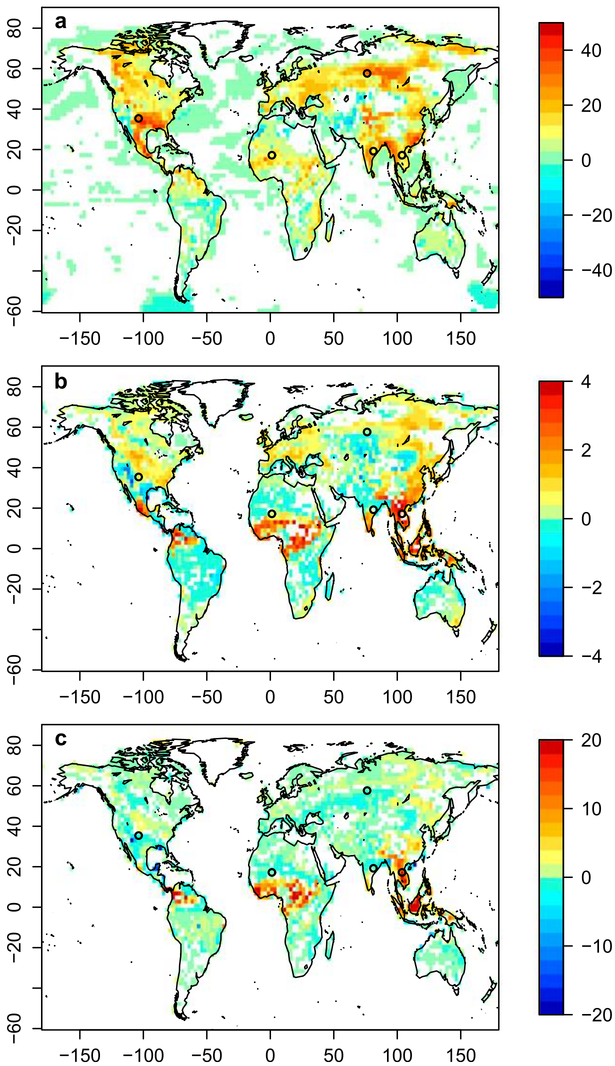

FIG. 5. Difference between (a) standard deviation ($\mathrm{W\,m^{-2}}$), (b) skewness, and (c) kurtosis of JJA daily sensible heat flux simulations CTL and 1A over 1971–2000. Pixels with no significant difference are blanked out, as in Fig. 1. Note that for kurtosis in (c), the color scale saturates at −20–+20 for greater legibility. Panels (b) and (c) are shown over land only.

is enhanced from 1A to CTL over some regions (e.g., central Asia) and may thus play a role in the changes of the temperature distribution, no clear relationship emerges at the global scale between changes in incoming solar radiation variability (or its higher-order moments) and temperature (not shown). Thus, on the global scale, feedbacks of turbulent heat fluxes to cloud cover and radiation do not appear to contribute largely to the change in surface temperature variability or higher-order moments.

c. *Time scale of variability*

By comparing simulations with prescribed and interactive soil moisture, we have demonstrated that soil moisture–atmosphere interactions strongly influence the distribution of daily summertime surface temperatures over land in GFDL ESM2M. One important aspect of temperature variability that is not characterized by the associated PDFs, however, is the time scale of variability, in particular, that changes in daily temperature distributions may reflect changes in variability across distinct time scales—that is, daily-to-interannual time scales (e.g., Fischer and Schär 2009).

As a first step to investigate the temporal characteristics, Fig. 6 decomposes the difference in temperature standard deviation between CTL and 1A (shown on Fig. 1b) into two time scales of interest in land–atmosphere coupling, synoptic and interannual. Note that the mean seasonal cycle of temperature is now removed from each simulation, and the resulting anomalies are bandpass filtered to retain the variability corresponding to periods of either 1–5 days (Fig. 6a) or >360 days (Fig. 6b). Figure 6 clearly illustrates that over different regions, soil moisture–atmosphere interactions enhance temperature variability on different time scales. Over central Asia, the increase in temperature variability is most strongly evident at synoptic time scales (a few days), whereas over three of the other areas highlighted (India, the Sahel, and the southern United States), temperature variability is mostly enhanced on interannual time scales. In terms of temperature PDFs, this means that the high-side tail of the multiyear, daily temperature distribution in CTL over central Asia shown on Fig. 2 is populated by short time scale fluctuations occurring every summer as a result of interactive soil moisture, whereas over India, the Sahel, and the southern United States, the tails of the temperature distribution are largely filled by days in particular summers that are anomalously cold or warm seasonally.

Figures 6c and 6d show that sensible heat flux variability is also enhanced more strongly with interactive soil moisture at synoptic relative to interannual time scales over Asia, although the separation of time scales is less distinct than for temperature. Over the other regions examined, the opposite is true. This is consistent with soil moisture–atmosphere interactions generating temperature variability at different time scales over different regions, as in Figs. 6a,b.

Neglect of the mean temperature seasonal cycle in Fig. 6 potentially obscures important impacts of soil moisture dynamics on seasonality (Teuling et al. 2006). To remedy this, Fig. 7 illustrates the mean seasonal cycle over the five representative points analyzed in section 3. One can see that over North America and central Asia, the increase in mean temperature between 1A and CTL is not a uniform shift throughout the year but is associated with a strongly enhanced seasonal cycle. In particular, the

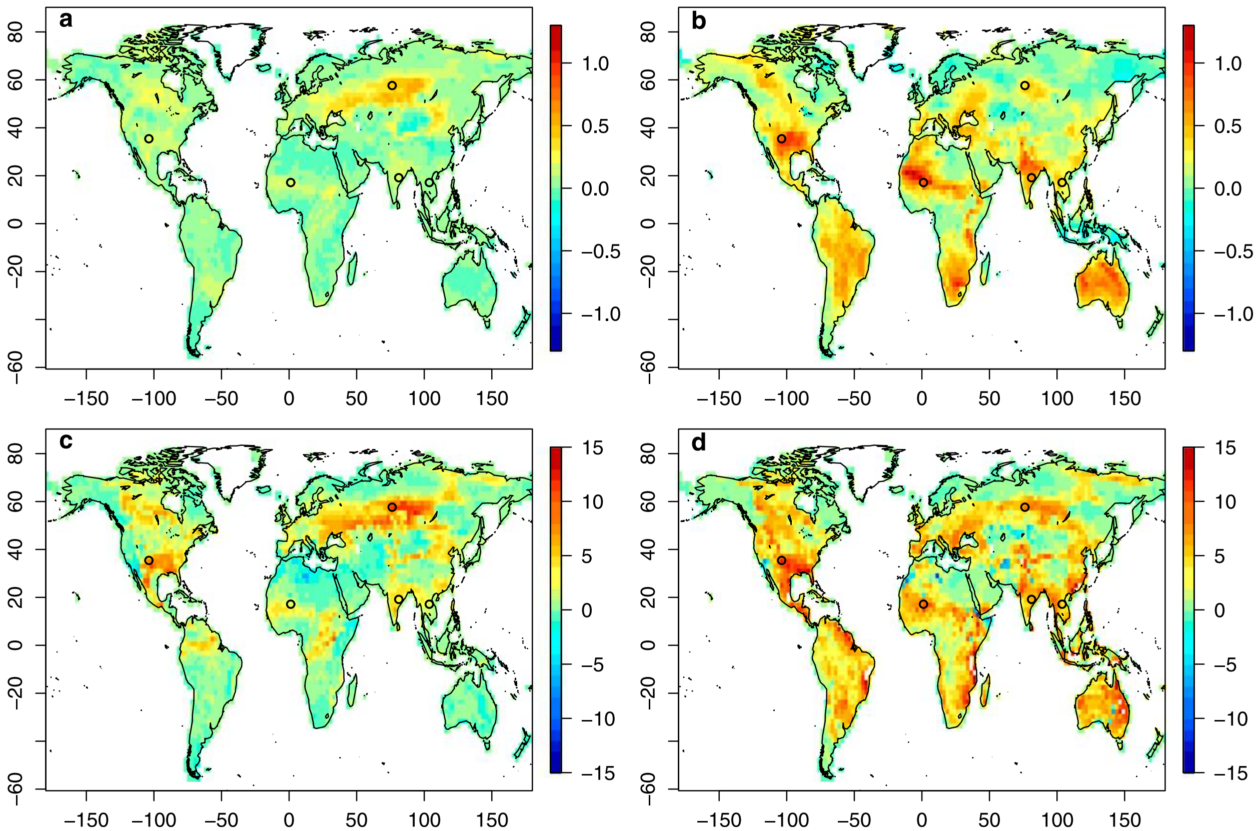

FIG. 6. Difference between standard deviation of JJA daily 2-m temperature anomalies (K) between simulations CTL and 1A over 1971–2000 over land, retaining only the variability (a) between 1 and 5 days and (b) above 360 days. (c),(d) As in (a),(b), but for daily sensible heat flux anomalies (W m^{-2}), respectively.

increase in temperature is maximized at the peak of the seasonal cycle, which reflects the asymmetric effect of interactive soil moisture on the temperature PDF (i.e., warm conditions are disproportionately impacted compared to cool conditions). Figure 7 shows that the differences in temperature seasonality between CTL and 1A throughout JJA can be interpreted in terms of the seasonalities of latent and sensible heating. This enhanced temperature seasonality contributes to the increase in daily variability, as well as to other changes in higher-order moments of the daily temperature distribution over these regions. In other words, the increase in daily variability corresponds to increasing seasonal cycle amplitude (Fig. 7) and increased amplitude of the anomalies relative to the seasonal cycle at daily time scales mostly over central Asia and at interannual time scales mostly over North America (Figs. 6a,b). Over the other regions, the seasonal cycle is less affected in JJA.

Ultimately, we suggest that the distinct regional impacts of soil moisture dynamics on temperature variability at different time scales are associated with different time scales of precipitation variability, and thus soil moisture variability, over these regions. For instance, Fig. 8 shows that soil moisture varies much more at interannual time scales over the Southeast United States than over central Asia. In general, the southeast United States, West Africa, and India lie at lower latitudes and closer to the oceanic moisture sources than central Asia, so summertime precipitation variability in these regions is arguably more affected by sea surface temperature interannual variability (e.g., ENSO). Interestingly, in this context, Fig. 6 suggests that interannual temperature variability associated with SST variations is only fully expressed in the model if soil moisture dynamics are included. In other words, the reduced interannual temperature variability in 1A (Fig. 6b) indicates that at least part of temperature interannual variability in the control run is the result of the soil moisture–mediated anticorrelation between precipitation and temperature. Together with the simulations analyzed here, additional simulations using prescribed climatological SSTs instead of time-varying SSTs should provide a more complete framework to tease apart the origins of temperature variability over different regions in the model (e.g., Koster et al. 2000).

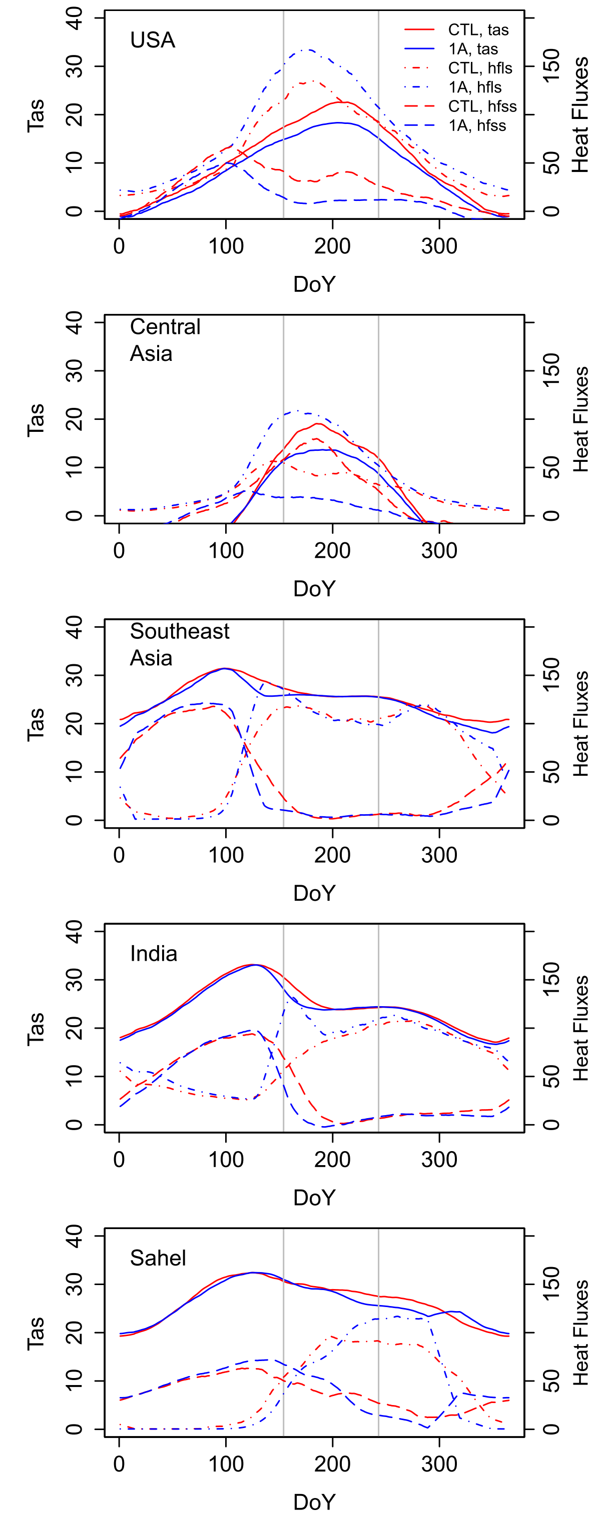

FIG. 7. (top to bottom) Over same five points as Figs. 2 and 3, mean seasonal cycle over 1971–2000 of 2-m temperature (full lines; left y axis; in °C), latent heat flux (hfls; dashed–dotted lines; right y axis; in W m^{-2}), and sensible heat flux (hfss; dashed lines; right y axis; in W m^{-2}) for CTL (red) and 1A (blue). Day of year (DoY) is on the x axis. Vertical gray lines delimit JJA.

4. Discussion and conclusions

One obvious limitation of our study is that our results are based on analysis of a single model. The impact of soil moisture dynamics on temperature distributions is related to the strength of soil moisture–atmosphere coupling in the model, and previous studies have shown that land–atmosphere coupling can vary largely between models (e.g., Koster et al. 2006; Seneviratne et al. 2010). Other models might thus yield different results regarding the impact of soil moisture variability on temperature distributions. As a first step to increase the robustness of the results presented here and assess the spread between climate models in terms of soil moisture impacts on temperature distribution, one could investigate simulations from the other models participating in the GLACE-CMIP5 experiment. Such an investigation was beyond the scope of the present study (only GFDL ESM2M simulations were available at the time of analysis); however, we point out here that, as mentioned in the introduction, comparing temperature distributions between models may prove challenging, as grid cell scale PDFs cannot be readily visualized and compared on the global scale across models. Recently Loikith et al. (2013) presented a PDF clustering methodology allowing for the comparison of climate distribution across datasets, which could be useful for model intercomparison. Alternatively, analysis of distribution moments, as in the present study, can provide a first-order basis for comparison. In general, we propose that some elements of analysis presented here—changes in different moments of distribution, time scales of change in variability—be considered in further studies of land–atmosphere coupling, as we showed that some usual diagnostics (e.g., change in daily standard deviation) might conceal impacts on other moments or time scales of variability.

One irreducible limitation associated with the experimental setup used in this study in agreement with the GLACE-CMIP5 protocol is that simulation 1A is a highly idealized experiment in which overriding soil moisture by the climatological seasonal cycle introduces some physical inconsistencies. In particular, overriding soil moisture in this way disrupts the water cycle, as the model is no longer required to conserve water. Over certain regions, it essentially provides a spurious source of latent heat at the surface (e.g., central Asia); enhanced evapotranspiration without soil moisture depletion (since soil moisture is overridden at each model time step) then leads to the net creation and input of water to the atmosphere. Note that since the atmosphere cannot store this additional water, precipitation also increases (by up to 2 mm day^{-1} in 1A) as a result of

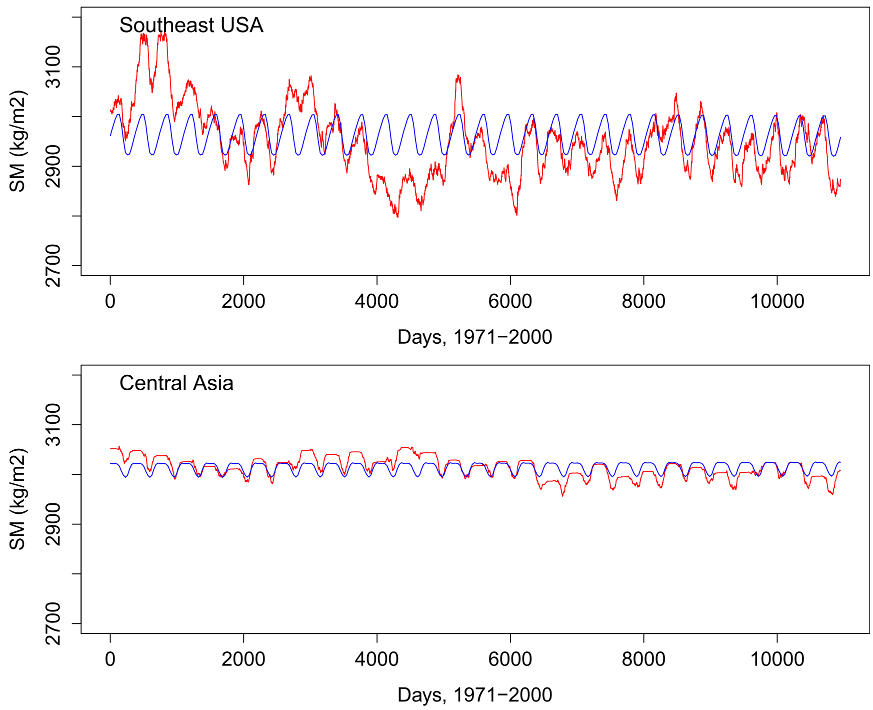

FIG. 8. Daily total soil moisture (SM) over 1971–2000, taking the mean over regional boxes over (top) the Southeast United States (108.75°–83.75°W, 31.3°–39.4°N) and (bottom) central Asia (53.75°–103.75°E, 49.5°–63.7°N) in simulations CTL (red) and 1A (blue).

increased land evapotranspiration and cloud cover (not shown); however, the increase in precipitation in 1A does not further feed back onto evapotranspiration and surface latent cooling, since soil moisture is prescribed in this simulation and does not respond to precipitation (the additional precipitation thus essentially disappears from the system again as it enters the ground). We saw in section 3b(2) that this difference in mean surface fluxes between 1A and CTL over certain regions is enhanced by the fact that a mean climatological distribution of soil moisture is prescribed in 1A, with large differences from the interactive soil moisture distribution. While there is arguably no perfectly physically consistent way to disable a physical process in a climate model (i.e., here, to design an experimental protocol turning off soil moisture–atmosphere interactions), alternative protocols could be considered that may minimize the disruption of the water cycle and thus the associated impacts on the mean climate: for instance, prescribing in simulation 1A one realization of soil moisture from the interactive simulation (either one year repeatedly or the whole multiannual, transient field), as was done at the seasonal time scale in the first GLACE experiment (Koster et al. 2004). While water would not be conserved in such a setup either, this would permit the inclusion of a similar PDF of soil moisture between both simulations, thus possibly limiting the disruption of the water cycle while still disabling soil moisture–atmosphere interactions. Alternatively, one could prescribe directly the seasonal cycle of surface heat fluxes instead of soil moisture, thus disabling soil moisture–atmosphere interactions by breaking the link between soil moisture and surface fluxes instead of breaking the link between precipitation and soil moisture (e.g., Koster et al. 2000; Reale and Dirmeyer 2002; Schubert et al. 2004). An interesting question is whether these different ways of severing the feedback loop between soil moisture and surface climate would yield similar results regarding the impact of these processes on surface temperature distributions. Krakauer et al. (2010), for instance, following the same protocol as in the present study (i.e., prescribing soil moisture climatology), note that the impact of soil moisture dynamics on the mean evapotranspiration and precipitation over land in their study is of the opposite sign of that in Reale and Dirmeyer (2002), in which surface fluxes rather than soil moisture are prescribed using a constant evaporative efficiency or ratio of actual to potential evapotranspiration. One may thus anticipate differences in impacts on higher-order moments of surface climate distributions (e.g., evapotranspiration and temperature) as well.

Our results also indicate that inclusion of dynamic vegetation strongly modulates the effect of prescribing

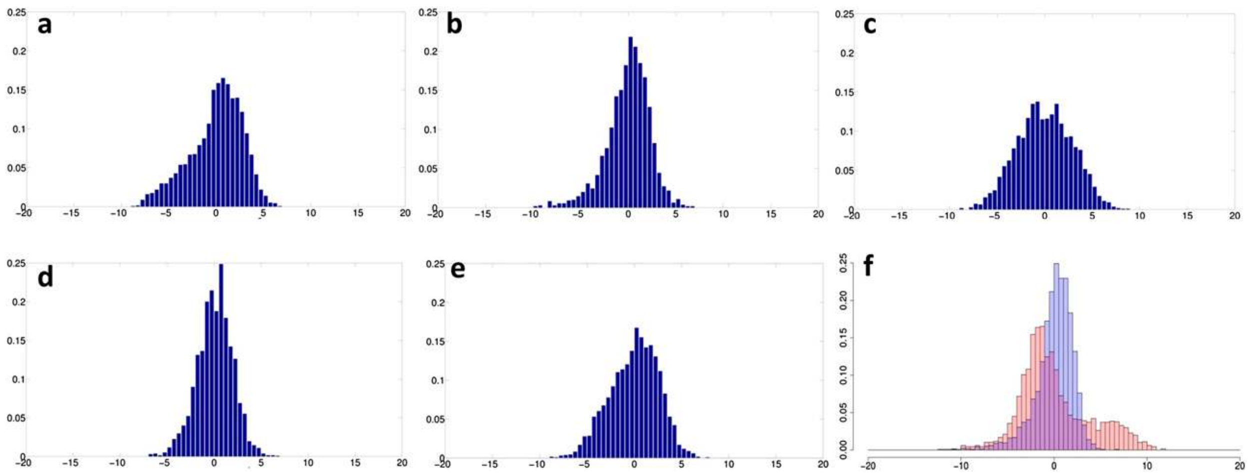

FIG. 9. Distribution of daily JJA temperature anomalies (K) over the North America pixel used in Figs. 2 and 3 (a) in NCEP-1 over 1971–2000; (b) in the North American Regional Reanalysis (NARR; Mesinger et al. 2006) over 1979–2002; (c) in the Modern-Era Retrospective Analysis for Research and Applications (MERRA; Rienecker et al. 2011) over 1979–2002; (d) in HadGHCND over 1971–2000; (e) in station data from Albuquerque [National Climate Data Center Global Summary of the Day (GSOD)] over 1971–2000; and (f) from simulations CTL (red) and 1A (blue). Differences between (f) and Fig. 2 reflect the difference between temperature anomalies and absolute values. The *y* axes show histogram densities.

soil moisture climatology in GFDL ESM2M [cf. section 3b(1)], in contrast to prior studies (e.g., Koster et al. 2006; Seneviratne et al. 2006; Krakauer et al. 2010) in which vegetation was nondynamic. This underscores how the effects of a particular experimental protocol may also depend on model configuration. Overall, we emphasize that analyzing the impact of soil moisture variability on surface climate by comparing interactive versus climatological soil moisture simulations is not strictly equivalent to isolating the contribution of soil moisture–atmosphere interactions: the former is an operational protocol, amongst others, to achieve insight into the more conceptual notion of the latter. We note that the GLACE-CMIP5 protocol was introduced mainly to investigate the impact of mean soil moisture change on climate in the context of long-term climate change (Seneviratne et al. 2013), rather than the role of soil moisture–atmosphere interactions in present climate per se.

While the model experiment allows us here to probe the role of simulated soil moisture variability on temperature PDFs, observational validation of these results is obviously challenging, since there is no equivalent to the prescribed soil moisture simulation in nature. On the other hand, to the extent that the interactive soil moisture simulation is meant to represent the real climate system, we can compare observed temperature PDFs to the simulated ones. While extensive investigation is beyond the scope of the present study, a cursory analysis indicates that the temperature distributions show some striking disagreement between various observational [Hadley Centre Global Historical Climatology Network–Daily (HadGHCND); Caesar et al. (2006)] or observationally constrained datasets (i.e., various reanalyses; Fig. 9). Over the southern U.S. point used in this study, the shape of the temperature PDF varies considerably across datasets (comparable differences were evident at some of the other points). For reanalysis products in particular, we suggest that this reflects the lack of direct assimilation constraints on near-surface temperature. For example, surface temperature is a "class B" product in the National Centers for Environmental Prediction–National Center for Atmospheric Research reanalysis (NCEP-1) (Kalnay et al. 1996), which means that it is partially defined by observations but also strongly influenced by the reanalysis model characteristics. This may be especially critical for distribution moments beyond the mean or variance. We also point out differences between gridded observations (Fig. 9d) and collocated station data (Fig. 9e). In this context, it is difficult to validate temperature PDFs from our simulations.

However, the much greater skewness in the CTL simulation compared to observations (see Fig. 9f) appears to indicate overestimation of soil moisture–atmosphere coupling strength in GFDL ESM2M. In previous GLACE intercomparisons, an earlier version of the GFDL model using the same atmospheric component (albeit with a different land model) did indeed exhibit strong land–atmosphere coupling compared to many of the other models in the GLACE ensemble (Koster et al. 2004, 2006), and preliminary results from GLACE-CMIP5 models also indicate a greater enhancement of summer temperature interannual variability in CTL compared to 1A in the GFDL model, which suggests a greater coupling strength in this model. However, such a comparison between observations and simulation CTL cannot by itself rule out the existence of a contribution of soil moisture dynamics to temperature distributions in nature physically similar to the one implied by the present study.

We also comment on the potentially critical role of higher-order moments of surface temperature and their link to soil moisture for data assimilation. In pioneering work, Mahfouf (1991) demonstrated how assimilation of screen-level temperature could improve soil moisture prediction since the daytime course of air temperature reflects surface energy partitioning at the surface within the land–boundary layer coupled system (Gentine et al. 2011). Since this work, air temperature has been used in some land surface data assimilation products (Bouttier et al. 1993a,b; Balsamo et al. 2007). Nonetheless, all current operational assimilation techniques (ensemble Kalman filter–smoother and 3D- and 4Dvar) rely on Gaussian assumption for the shape of the assimilated and observed variables. We have shown in this study that in many cases the variance and mean may be poor indicators of soil moisture impact on surface air temperature. This stresses the need to consider implementation of assimilation frameworks that are more sensitive to higher-order moments (van Leeuwen 2010).

Overall, by comparing simulations with prescribed and interactive soil moisture, we have shown how soil moisture–atmosphere interactions strongly influence the distribution of daily summertime surface temperature over land in a number of regions in GFDL EMS2M. Large changes in the mean and standard deviation of the temperature distribution were found to occur in well-known hotspot regions, in general agreement with previous modeling studies (e.g., Krakauer et al. 2010; Koster et al. 2006; Seneviratne et al. 2006). Beyond that, our results demonstrate that the shape of the temperature PDF, characterized by higher-order moments of the distribution, is also strongly modulated when soil moisture dynamics is suppressed. These changes mostly reflect the impact of stronger soil moisture control on evapotranspiration in the interactive simulation, which is associated with positive sensible heat flux anomalies that lead to higher temperatures. Importantly, the different temperature PDF parameters are not all affected at the same time or in a similar way in different regions. We interpret these different impacts as arising from geographic variation in mean hydroclimate and rainfall characteristics and how interactive soil moisture affects the distribution of soil moisture anomalies, and thus of surface fluxes, over these regions. For instance, over the drier southern United States and central Asia, the positively skewed soil moisture distribution in the simulation with interactive soil moisture leads to a strong decrease in average evapotranspiration and increase in mean temperature; on the other hand, over the wetter Southeast Asia or West Africa, negatively skewed soil moisture anomalies induce relatively few low evapotranspiration anomalies and thus a sharp tail in high sensible heat flux and temperature anomalies, associated with a strong increase in skewness but little other change in the distribution. These different behaviors underscore the importance of analyzing more than the first two distribution moments to characterize the impacts of soil moisture–atmosphere interactions on surface temperature. In particular, some effects might be poorly captured by changes in the standard deviation alone. Our results also underscore the need to consider data assimilation techniques with non-Gaussian assumptions to estimate soil moisture.

In our model, the general effect of soil moisture dynamics and associated feedbacks to the atmosphere is to increase the variance, increase the skewness, and decrease the kurtosis of the temperature distribution. As a result, soil moisture–atmosphere interactions strongly contribute to shaping the high-side tail of the temperature PDF. The results also indicate that these effects might take place at different time scales over different regions. Overall, these results suggest the feedbacks to the atmosphere associated with soil moisture dynamics are critical for summertime high temperature extremes. This study thus contributes to the growing body of work linking climate PDFs, climate extremes, and physical processes; our results suggest a correct representation of land–atmosphere coupling is essential to the simulation of summer temperature extremes in the present climate, as well as to an understanding of how such extremes are projected to change in a future, warmer climate.

Acknowledgments. This work was supported by National Science Foundation (NSF) Grants AGS-1035968 and AGS-1035843 and New Jersey Agricultural Experiment Station Hatch Grant NJ07102. A.B. is currently supported by NSF Postdoctoral Fellowship AGS-1331375. S.M. acknowledges support from the National Oceanic and Atmospheric (U.S. Department of Commerce) Grant NA08OAR4320752, U.S. Department of Agriculture Grant 2011-67003-30373, and the Carbon Mitigation Initiative at Princeton University, sponsored by British Petroleum. Part of this research was carried out at the Jet Propulsion Laboratory, California Institute of Technology, under a contract with the National Aeronautics and Space Administration. The authors thank Sonia Seneviratne for her comments on the manuscript.

REFERENCES

Ballester, J., F. Giorgi, and X. Rodo, 2010: Changes in European temperature extremes can be predicted from changes in PDF central statistics: A letter. *Climatic Change,* **98,** 277–284, doi:10.1007/s10584-009-9758-0.

Balsamo, G., J. Mahfouf, S. Bélair, and G. Deblonde, 2007: A land data assimilation system for soil moisture and temperature: An information content study. *J. Hydrometeor.,* **8,** 1225–1242, doi:10.1175/2007JHM819.1.

Betts, A. K., 2007: Coupling of water vapor convergence, clouds, precipitation, and land-surface processes. *J. Geophys. Res.,* **112,** D10108, doi:10.1029/2006JD008191.

——, and P. Viterbo, 2005: Land-surface, boundary layer, and cloud-field coupling over the southwestern Amazon in ERA-40. *J. Geophys. Res.,* **110,** D14108, doi:10.1029/2004JD005702.

——, B. Helliker, and J. Berry, 2004: Coupling between CO_2, water vapor, temperature, and radon and their fluxes in an idealized equilibrium boundary layer over land. *J. Geophys. Res.,* **109,** D18103, doi:10.1029/2003JD004420.

Bouchet, R. J., 1963: Évapotranspiration réelle et potentielle: Signification climatique. *Proc. IASH General Assembly,* Berkeley, CA, International Association of Science and Hydrology, 134–142.

Bouttier, F., J. Mahfouf, and J. Noilhan, 1993a: Sequential assimilation of soil moisture from atmospheric low-level parameters. Part I: Sensitivity and calibration studies. *J. Appl. Meteor.,* **32,** 1335–1351, doi:10.1175/1520-0450(1993)032<1335:SAOSMF>2.0.CO;2.

——, ——, and ——, 1993b: Sequential assimilation of soil moisture from atmospheric low-level parameters. Part II: Implementation in a mesoscale model. *J. Appl. Meteor.,* **32,** 1352–1364, doi:10.1175/1520-0450(1993)032<1352:SAOSMF>2.0.CO;2.

Caesar, J., L. Alexander, and R. Vose, 2006: Large-scale changes in observed daily maximum and minimum temperatures: Creation and analysis of a new gridded data set. *J. Geophys. Res.,* **111,** D05101, doi:10.1029/2005JD006280.

Conil, S., H. Douville, and S. Tyteca, 2007: The relative influence of soil moisture and SST in climate predictability explored within ensembles of AMIP type experiments. *Climate Dyn.,* **28,** 125–145, doi:10.1007/s00382-006-0172-2.

Diffenbaugh, N. S., J. S. Pal, R. J. Trapp, and F. Giorgi, 2005: Fine-scale processes regulate the response of extreme events to global climate change. *Proc. Natl. Acad. Sci. USA,* **102,** 15 774–15 778, doi:10.1073/pnas.0506042102.

Dirmeyer, P. A., 2003: The role of the land surface background state in climate predictability. *J. Hydrometeor.,* **4,** 599–610, doi:10.1175/1525-7541(2003)004<0599:TROTLS>2.0.CO;2.

D'Odorico, P., and A. Porporato, 2004: Preferential states in soil moisture and climate dynamics. *Proc. Natl. Acad. Sci. USA,* **101,** 8848–8851, doi:10.1073/pnas.0401428101.

Donat, M. G., and L. V. Alexander, 2012: The shifting probability distribution of global daytime and night-time temperatures. *Geophys. Res. Lett.,* **39,** L14707, doi:10.1029/2012GL052459.

Dunne, J. P., and Coauthors, 2012: GFDL's ESM2 global coupled climate–carbon Earth System Models. Part I: Physical formulation and baseline simulation characteristics. *J. Climate,* **25,** 6646–6665, doi:10.1175/JCLI-D-11-00560.1.

Field, C. B., and Coauthors, Eds., 2012: *Managing the Risks of Extreme Events and Disasters to Advance Climate Change Adaptation*. Cambridge University Press, 582 pp. [Available online at http://ipcc-wg2.gov/SREX/images/uploads/SREX-All_FINAL.pdf.]

Findell, K. L., and E. A. B. Eltahir, 2003a: Atmospheric controls on soil moisture–boundary layer interactions. Part I: Framework development. *J. Hydrometeor.,* **4,** 552–569, doi:10.1175/1525-7541(2003)004<0552:ACOSML>2.0.CO;2.

——, and ——, 2003b: Atmospheric controls on soil moisture–boundary layer interactions. Part II: Feedbacks within the continental United States. *J. Hydrometeor.,* **4,** 570–583, doi:10.1175/1525-7541(2003)004<0570:ACOSML>2.0.CO;2.

——, P. Gentine, B. R. Lintner, and C. Kerr, 2011: Probability of afternoon precipitation in eastern United States and Mexico enhanced by high evaporation. *Nat. Geosci.,* **4,** 434–439, doi:10.1038/ngeo1174.

Fischer, E. M., and C. Schär, 2009: Future changes in daily summer temperature variability: Driving processes and role for temperature extremes. *Climate Dyn.,* **33,** 917–935, doi:10.1007/s00382-008-0473-8.

——, S. I. Seneviratne, D. Lüthi, and C. Schär, 2007: The contribution of land–atmosphere coupling to recent European summer heat waves. *Geophys. Res. Lett.,* **34,** L06707, doi:10.1029/2006GL029068.

Gentine, P., D. Entekhabi, and J. Polcher, 2010: Spectral behaviour of a coupled land-surface and boundary-layer system. *Bound.-Layer Meteor.,* **134,** 157–180, doi:10.1007/s10546-009-9433-z.

——, ——, and ——, 2011: The diurnal behavior of evaporative fraction in the soil–vegetation–atmospheric boundary layer continuum. *J. Hydrometeor.,* **12,** 1530–1546, doi:10.1175/2011JHM1261.1.

——, A. A. M. Holtslag, F. D'Andrea, and M. Ek, 2013: Surface and atmospheric controls on the onset of moist convection over land. *J. Hydrometeor.,* **14,** 1443–1462, doi:10.1175/JHM-D-12-0137.1.

GFDL Global Atmospheric Model Development Team, 2004: The new GFDL global atmosphere and land model AM2–LM2: Evaluation with prescribed SST simulations. *J. Climate,* **17,** 4641–4673, doi:10.1175/JCLI-3223.1.

Griffiths, G. M., and Coauthors, 2005: Change in mean temperature as a predictor of extreme temperature change in the Asia–Pacific region. *Int. J. Climatol.,* **25,** 1301–1330, doi:10.1002/joc.1194.

Hirschi, M., and Coauthors, 2011: Observational evidence for soil-moisture impact on hot extremes in southeastern Europe. *Nat. Geosci.,* **4,** 17–21, doi:10.1038/ngeo1032.

Hohenegger, C., P. Brockhaus, C. S. Bretherton, and C. Schär, 2009: The soil moisture–precipitation feedback in simulations with explicit and parameterized convection. *J. Climate,* **22,** 5003–5020, doi:10.1175/2009JCLI2604.1.

Jaeger, E. B., and S. I. Seneviratne, 2011: Impact of soil moisture–atmosphere coupling on European climate extremes and trends in a regional climate model. *Climate Dyn.,* **36,** 1919–1939, doi:10.1007/s00382-010-0780-8.

Kalnay, E., and Coauthors, 1996: The NCEP/NCAR 40-Year Reanalysis Project. *Bull. Amer. Meteor. Soc.,* **77,** 437–471, doi:10.1175/1520-0477(1996)077<0437:TNYRP>2.0.CO;2.

Koster, R. D., M. J. Suarez, and M. Heiser, 2000: Variance and predictability of precipitation at seasonal-to-interannual timescales. *J. Hydrometeor.,* **1,** 26–46, doi:10.1175/1525-7541(2000)001<0026:VAPOPA>2.0.CO;2.

——, P. A. Dirmeyer, A. N. Hahmann, R. Ijpelaar, L. Tyahla, P. Cox, and M. J. Suarez, 2002: Comparing the degree of land–atmosphere interaction in four atmospheric general circulation models. *J. Hydrometeor.,* **3,** 363–375, doi:10.1175/1525-7541(2002)003<0363:CTDOLA>2.0.CO;2.

——, and Coauthors, 2004: Regions of strong coupling between soil moisture and precipitation. *Science,* **305,** 1138–1140, doi:10.1126/science.1100217.

——, and Coauthors, 2006: GLACE: The Global Land–Atmosphere Coupling Experiment. Part I: Overview. *J. Hydrometeor.,* **7,** 590–610, doi:10.1175/JHM510.1.

Krakauer, N. Y., B. I. Cook, and M. J. Puma, 2010: Contribution of soil moisture feedback to hydroclimatic variability. *Hydrol. Earth Syst. Sci.,* **14,** 505–520, doi:10.5194/hess-14-505-2010.

Lin, S.-J., 2004: A ''vertically Lagrangian'' finite-volume dynamical core for global models. *Mon. Wea. Rev.,* **132,** 2293–2307, doi:10.1175/1520-0493(2004)132<2293:AVLFDC>2.0.CO;2.

Lintner, B. R., P. Gentine, K. L. Findell, F. D'Andrea, A. H. Sobel, and G. D. Salvucci, 2013: An idealized prototype for large-scale land–atmosphere coupling. *J. Climate,* **26,** 2379–2389, doi:10.1175/JCLI-D-11-00561.1.

Loikith, P. C., and A. J. Broccoli, 2012: Characteristics of observed atmospheric circulation patterns associated with temperature extremes over North America. *J. Climate,* **25,** 7266–7281, doi:10.1175/JCLI-D-11-00709.1.

——, B. R. Lintner, J. Kim, H. Lee, J. D. Neelin, and D. E. Waliser, 2013: Classifying reanalysis surface temperature probability density functions (PDFs) over North America with cluster analysis. *Geophys. Res. Lett.,* **40,** 3710–3717, doi:10.1002/grl.50688.

Mahfouf, J.-F., 1991: Analysis of soil moisture from near-surface parameters: A feasibility study. *J. Appl. Meteor.,* **30,** 1534–1547, doi:10.1175/1520-0450(1991)030<1534:AOSMFN>2.0.CO;2.

Mesinger, F., and Coauthors, 2006: North American Regional Reanalysis. *Bull. Amer. Meteor. Soc.,* **87,** 343–360, doi:10.1175/BAMS-87-3-343.

Milly, P., and Coauthors, 2014: An enhanced model of land water and energy for global hydrologic and earth-system studies. *J. Hydrometeor.,* **15,** 1739–1761, doi:10.1175/JHM-D-13-0162.1.

Miralles, D. G., M. J. vanden Berg, A. J. Teuling, and R. A. M. deJeu, 2012: Soil moisture–temperature coupling: A multiscale observational analysis. *Geophys. Res. Lett.,* **39,** L21707, doi:10.1029/2012GL053703.

Mueller, B., and S. I. Seneviratne, 2012: Hot days induced by precipitation deficits at the global scale. *Proc. Natl. Acad. Sci. USA,* **109,** 12 398–12 403, doi:10.1073/pnas.1204330109.

Neelin, J. D., B. R. Lintner, B. Tian, Q. Li, L. Zhang, P. K. Patra, M. T. Chahine, and S. N. Stechmann, 2010: Long tails in deep columns of natural and anthropogenic tropospheric tracers. *Geophys. Res. Lett.,* **37,** L05804, doi:10.1029/2009GL041726.

Orlowsky, B., and S. I. Seneviratne, 2010: Statistical analyses of land–atmosphere feedbacks and their possible pitfalls. *J. Climate,* **23,** 3918–3932, doi:10.1175/2010JCLI3366.1.

Paegle, J., K. C. Mo, and J. Nogués-Paegle, 1996: Dependence of simulated precipitation on surface evaporation during the 1993 United States summer floods. *Mon. Wea. Rev.,* **124,** 345–361, doi:10.1175/1520-0493(1996)124<0345:DOSPOS>2.0.CO;2.

Pal, J. S., and E. A. B. Eltahir, 2003: A feedback mechanism between soil-moisture distribution and storm tracks. *Quart. J. Roy. Meteor. Soc.,* **129,** 2279–2297, doi:10.1256/qj.01.201.

Reale, O., and P. Dirmeyer, 2002: Modeling the effect of land surface evaporation variability on precipitation variability. Part I: General response. *J. Hydrometeor.,* **3,** 433–450, doi:10.1175/1525-7541(2002)003<0433:MTEOLS>2.0.CO;2.

Rhines, A., and P. Huybers, 2013: Frequent summer temperature extremes reflect changes in the mean, not the variance. *Proc. Natl. Acad. Sci. USA,* **110,** E546, doi:10.1073/pnas.1218748110.

Rienecker, M. M., and Coauthors, 2011: MERRA: NASA's Modern-Era Retrospective Analysis for Research and Applications. *J. Climate,* **24,** 3624–3648, doi:10.1175/JCLI-D-11-00015.1.

Ruff, T. W., and J. D. Neelin, 2012: Long tails in regional surface temperature probability distributions with implications for extremes under global warming. *Geophys. Res. Lett.,* **39,** L04704, doi:10.1029/2011GL050610.

Schubert, S. D., M. J. Suarez, P. J. Pegion, R. D. Koster, and J. T. Bacmeister, 2004: Causes of long-term drought in the U.S. Great Plains. *J. Climate,* **17,** 485–503, doi:10.1175/1520-0442(2004)017<0485:COLDIT>2.0.CO;2.

Seneviratne, S. I., D. Lüthi, M. Litschi, and C. Schär, 2006: Land–atmosphere coupling and climate change in Europe. *Nature,* **443,** 205–209, doi:10.1038/nature05095.

——, T. Corti, E. L. Davin, M. Hirschi, E. B. Jaeger, I. Lehner, B. Orlowsky, and A. J. Teuling, 2010: Investigating soil moisture–climate interactions in a changing climate: A review. *Earth-Sci. Rev.,* **99,** 125–161, doi:10.1016/j.earscirev.2010.02.004.

——, and Coauthors, 2012: Changes in climate extremes and their impacts on the natural physical environment. *Managing the Risks of Extreme Events and Disasters to Advance Climate Change Adaptation,* C. B. Field et al., Eds., Cambridge University Press, 109–230.

——, and Coauthors, 2013: Impact of soil moisture–climate feedbacks on CMIP5 projections: First results from the GLACE-CMIP5 experiment. *Geophys. Res. Lett.,* **40,** 5212–5217, doi:10.1002/grl.50956.

Shevliakova, E., and Coauthors, 2009: Carbon cycling under 300 years of land use change: Importance of the secondary vegetation sink. *Global Biogeochem. Cycles,* **23,** GB2022, doi:10.1029/2007GB003176.

Simolo, C., M. Brunetti, M. Maugeri, and T. Nanni, 2011: Evolution of extreme temperatures in a warming climate. *Geophys. Res. Lett.,* **38,** L16701, doi:10.1029/2011GL048437.

Teuling, A. J., S. I. Seneviratne, C. Williams, and P. A. Troch, 2006: Observed timescales of evapotranspiration response to soil moisture. *Geophys. Res. Lett.,* **33,** L23403, doi:10.1029/2006GL028178.

van Leeuwen, P. J., 2010: Nonlinear data assimilation in geosciences: An extremely efficient particle filter. *Quart. J. Roy. Meteor. Soc.,* **136,** 1991–1999, doi:10.1002/qj.699.